


 Cite this: *New J. Chem.*, 2021, 45, 12120

Palladium supported on structurally stable phenanthroline-based polymer nanotubes as a high-performance catalyst for the aqueous Suzuki–Miyaura coupling reaction†

 Didi Yang,‡ Shuhui Wang,‡ Ting Dan, Dashuang Gao, Chaktong Au, Wanju Zhang* and Yan Zhang *

Though the Suzuki–Miyaura coupling reaction has intrinsic advantages in organic synthesis, it is still a challenging task to develop a highly active and truly heterogeneous catalyst for the aqueous Suzuki–Miyaura coupling reaction (SMR). In this work, a series of phenanthroline-based polymers (PBPs; PBP1 to PBP8) were synthesized by a simple one-step AlCl_3 -catalyzed Friedel–Crafts polymerization method. Systematic measurements of PBPs by N_2 adsorption–desorption isotherms, scanning electron microscopy (SEM), transmission electron microscopy (TEM), Fourier transform infrared spectroscopy (FT-IR) and thermogravimetric analysis (TGA) show that most of the PBPs have a nanosheet morphology, except PBP8 which has both one-dimensional nanotubular morphology and large surface area ($745 \text{ m}^2 \text{ g}^{-1}$). Benefitting from the porous nanotube morphology and the two N atoms contained in the phenanthroline unit of the polymer structure, polymer PBP8 shows adsorption effects and strong chelating stabilization on the Pd active metal (size, 2–5 nm). The Pd/PBP8 catalyst exhibits superior catalytic activity within 2 h (TOF value: 3077 h^{-1}) and reusability (7 cycles) in the SMR with typical reactants such as bromobenzene, phenylboronic acid and the base of $\text{K}_3\text{PO}_4 \cdot 3\text{H}_2\text{O}$ at $30 \text{ }^\circ\text{C}$ in a solvent mixture of water and ethanol ($V_{\text{H}_2\text{O}} : V_{\text{ethanol}} = 3 : 2$).

 Received 3rd October 2020,
 Accepted 29th April 2021

DOI: 10.1039/d0nj04864j

rsc.li/njc

1. Introduction

The design of materials with special morphologies and functions at the molecular level to achieve a green and sustainable synthesis of materials has become an important topic in research fields^{1–4} such as catalysis,^{5–7} gas capture^{8,9} and energy storage.^{10–12} By means of bottom-up polymerization strategies, porous polymer materials can be tailored into designated micro-morphologies.^{5,13–15} In particular, tubular polymer materials have attracted wide attention due to their special nanofiber morphology, large specific surface area ($> 600 \text{ m}^2 \text{ g}^{-1}$), structure adjustability (polymer structure could be changed by replacing its structural units with other organic units) and functional diversity (including adsorbed gas, catalyst supporter, energy storage, etc.).^{6,9,16–18} Nonetheless, it is not easy to synthesize tubular polymer materials. This involves harsh polymerization conditions, including diversity of monomers (such as porphyrin,

ethynylarenes, haloarenes, benzyl halide, and so on),^{7,16} well-designed templates (SiO_2),¹¹ and expensive Pd(0) or Pd(II) catalysts.^{7,19}

For example, Zhao, *et al.*¹¹ synthesized a tube-in-tube structured carbon nanomaterial by coating acid-treated multiwalled carbon nanotubes with porous SiO_2 layers, which was designed as the template for trapping octadecyltrimethoxysilane (C_{18}TMS). After C_{18}TMS was converted into carbon within the porous SiO_2 *via* chemical treatment and high-temperature calcinations, a tube-in-tube carbon nanostructure was obtained by etching the SiO_2 layer with NaOH solution. The synthesis strategy of the tube-in-tube structured carbon nanomaterial involves hard templates and a high-temperature carbonization process, which could be interminable. Zhu, *et al.*⁷ synthesized nanotube-like porphyrin-based polymers as nanoporous nitrogen-rich metal-free electrocatalysts using a one-step cross-coupling reaction under the condition of noble metal Pd(0)/CuI as the catalyst. Chun, *et al.*¹⁹ reported a tubular-shape microporous organic network, which was synthesized in need of the noble metal catalyst PdCl_2/CuI . Compared with the above methods, the one-step AlCl_3 -catalyzed Friedel–Crafts polymerization reaction has the advantages of simple synthesis and cheap and easily available non-precious metal salt catalysts.

Hubei Key Laboratory for Processing and Application of Catalytic Materials,
 Huanggang Normal University, Huanggang 438000, China.

E-mail: wanjuzhang@126.com, zhangyan@hgnu.edu.cn

† Electronic supplementary information (ESI) available. See DOI: 10.1039/d0nj04864j

‡ Both authors have contributed equally to this work.

Tubular polymeric materials with extra functionalities can be fabricated by adjusting the physicochemical properties of original polymeric nanotubes by means of heteroatom modification.^{20–24} For instance, introducing phenolic hydroxyls into the skeleton of nanotube-like organic porous materials could improve the hydrophilic performance, which in turn improves the adsorption performance of amphiphilic-hydrophilic organics in the water phase.^{4,11,25–27} The introduction of pyrrolic nitrogen into the framework of hollow copolymer tubes could enhance the adsorption selectivity of small functional peptides.^{1,28} The doping of catechol in porous polymers could enhance the cycling stability and provide Lewis acid active sites in a Fe catalyst.^{5,29} Besides, it is reported that heteroatomic organic ligands in polymer materials are beneficial to the adsorption of metal nanoparticles.^{30–33} Moreover, the SMR reaction system is composed of lipophilic aromatic halogen derivatives, hydrophilic phenylboronic acid derivatives, water-soluble basic inorganic salts and a Pd catalyst. There are two advantages of introducing heteroatoms into tubular polymeric materials: (1) anchoring the active Pd nanoparticles and (2) enhancing the interactions of the compounds in the SMR reaction system.³⁴ Since the pincer-like nitrogen and chelating structure in 1,10-phenanthroline ligands have strong coordination ability with metal nanoparticles, phenanthroline-based organic porous materials (POPMS) show excellent catalytic performance in heterogeneous catalysis.^{33,35–37} Due to the multiple reaction sites in the Friedel-Crafts polymerization reaction, it is difficult for phenanthroline monomers to form a long-range ordered structure like inorganic materials, and the phenanthroline-based polymers mainly showed random block shapes and rare ordered morphology.^{33,35–37} Currently, it is difficult to synthesize POPMS with a nanotube morphology.

So far, heteroatoms (nitrogen and oxygen) have been successfully doped into the framework of tubular polymers,^{16,19,38–40} showing a large surface area. Nevertheless, mostly tubular polymers were synthesized by using a tedious template method,^{16,38} multi-step reactions,³⁹ and a noble metal catalyst.^{19,40} In this work, a new type of 1,10-phenanthroline-based tubular polymer was easily synthesized through a one-step Friedel-Crafts polymerization reaction with a non-noble metal catalyst AlCl_3 . When used as a support for Pd-catalyzed SMRs, the Pd nanoparticles (2–5 nm) are dispersed in the tubular polymer support, and the tubular polymer support catalyst Pd/PBP8 displayed excellent selectivity, activity, and recyclability.

2. Experimental

2.1 Preparation of PBPs and TMP

As depicted in Fig. 1, all 1,10-phenanthroline-based polymer (PBP) materials were synthesized by the AlCl_3 -catalyzed Scholl reaction^{1,13,41–44} of 1,10-phenanthroline with a series of aromatic co-monomers in CH_2Cl_2 solvent, and the preparation details are provided in Table S1 of the ESI.† In a typical synthesis, 0.793 g of 1,10-phenanthroline monohydrate monomer, 0.641 g of

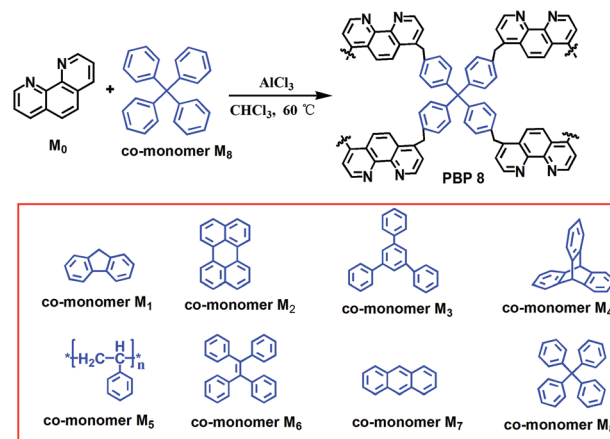


Fig. 1 Schematic for the synthesis of 1,10-phenanthroline-based materials.

tetraphenylmethane and 30 mL of CH_2Cl_2 were added into an eggplant flask and stirred at 600 rpm for 30 minutes at room temperature to form a homogenous solution. Under the protection of argon, 3.206 g of anhydrous AlCl_3 was added to the above solution, and the mixture was heated to 60 °C and stirred at 600 rpm for 48 h. After cooling to room temperature, the collected precipitate was first washed with 15 mL of 2 M HCl and then with 100 mL of ethanol. Finally, the residual AlCl_3 was removed by subsequent washing with ethanol, tetrahydrofuran and methylene dichloride for 24 h using a Soxhlet extractor. The final solid product was dried in a vacuum oven to give a brown powder (yield: 96%), which is herein named PBP8. Similarly, phenanthroline-based polymers PBP1, PBP2, PBP3, PBP4, PBP5, PBP6, and PBP7 were synthesized following the steps for the synthesis of PBP8 but adopting fluorene (0.333 g), perylene (0.505 g), 1,3,5-triphenylbenzene (0.817 g), triptycene (0.678 g), poly(styrene) (0.832 g), tetraphenylethylene (0.665 g), and anthracene (0.357 g) as co-monomers, respectively.

At the same time, TMP was synthesized from tetraphenylmethane and phenanthrene *via* the same synthesis steps of PBP8.

2.2 Synthesis of the PBP8-supported Pd catalyst

With many aromatic rings and pyridinic nitrogen atoms in the skeleton of 1,10-phenanthroline-based polymers, the as-synthesized materials are endowed with hydrophilic and lipophilic properties. Consequently, the 1,10-phenanthroline-based polymer materials can be dispersed in polar organic solvents. The PBP8-supported Pd catalyst was prepared in acetonitrile solution with strong polarity. In a typical run, 0.100 g of palladium chloride powder and 30 drops of concentrated HCl were dissolved into 30 mL of acetonitrile to obtain a clear solution. Next, 1.000 g of PBP8 material was dispersed into the above solution and the mixture was heated at 70 °C in a round bottom flask for 12 h under Ar atmosphere. Finally, the solid was filtered out and rinsed with dichloromethane in a Soxhlet extractor for 24 h to remove the poorly adsorbed PdCl_2 , and then dried in a vacuum oven at 50 °C for 12 h to obtain the

supported Pd catalyst. The acquired catalyst is herein named Pd/PBP8. The loading of Pd in the corresponding catalyst is 0.14 wt%, which was measured by atomic absorption spectroscopy.

2.3 Characterization of materials

The porosity, microstructure, thermal stability and other properties of PBP and TMP materials were investigated by Fourier transform infrared spectroscopy (FT-IR), thermogravimetric analysis (TGA), scanning electron microscopy (SEM), transmission electron microscopy (TEM), and N₂ adsorption–desorption isotherms. Among the prepared PBPs, PBP8 is the only material that has the features of both nanotube morphology and large specific surface area. Hence, polymer nanotube PBP8 was selected as the support for the loading of Pd (Pd/PBP8 catalyst) to catalyze SMRs. The Pd/PBP8 catalyst was investigated by SEM, TEM, N₂ adsorption–desorption isotherms and X-ray photoelectron spectroscopy (XPS). The Pd contents on both the fresh Pd/PBP8 and Pd/TMP catalysts were analysed by measuring the precursor solutions of the Pd-loaded catalysts using atomic absorption spectroscopic analysis (AAS) and the Pd contents in the reaction mother liquids after the solid catalysts are removed from the Suzuki reaction were analysed by inductively coupled plasma-optical emission spectroscopy (ICP-OES).

2.4 General procedure for Suzuki–Miyaura reaction (SMR)

In a typical run, arylborane compound (0.75 mmol), base (1.50 mmol) and Pd/PBP8 (4.9 mg, n_{Pd}:n_{aryl halide} = 0.00013:1) catalyst were dispersed in 3 mL of a solvent in a 10 mL brown glass sample bottle with PP cap and stirred with the rate of 600–700 rpm for 10 min to achieve a uniform dispersion, and then aryl halide (0.5 mmol) was added to the above dispersion to start the SMR. The progress of the reaction was monitored using TLC plates, in which petroleum ether was used as the solvent at room temperature. The activity of the Pd/PBP8 is the isolated yield, which is the ratio of the actual mass of the product separated by the TLC plates to the theoretical mass of the complete transformation of the reactants.

2.5 Hot filtration experiment

The hot filtration experiment was conducted by the reported method,⁴⁵ which was used to prove that the catalyst is a heterogeneous catalyst. After the reaction of bromobenzene and phenylboronic acid under optimal conditions for 0.5 h, 0.2 mL of the reaction liquid was taken to analyze the yield after the removal of the heterogeneous catalyst by filtration. The mother liquid was allowed to react continuously under the same conditions for another 3 h and then the yield was analyzed again. Then, the Pd concentrations in the reaction mother liquids were analysed by ICP-OES. The hot filtration experiment was performed in three-fold.

2.6 Recycling experiment for the SMR of bromobenzene with phenylboronic acid

After the coupling reaction of bromobenzene and phenylboronic acid, the Pd catalyst was separated by filtration from the reaction

system, and the corresponding activity was measured using a GC9790-II gas chromatograph (Fuli GC9790-II, Zhejiang analytical instrument Inc., China) with naphthalene (0.5 mmol) as an external standard. The products in the effluent were analyzed using a flame ionization detector (FID) and an appropriate column (HP-5, China) using a nitrogen carrier gas. The analysis was performed under the condition that the temperature was maintained at 80 °C for 3 minutes and then was heated to 260 °C (at the rate of 15 °C min⁻¹) and maintained for 3 min. The collected catalyst was washed with *ca.* 50 mL of deionized water and 50 mL of ethanol to remove impurities, and then dried in a vacuum oven at 50 °C for 12 h before being used for the next cycle.

3. Results and discussion

The pore structures of PBPs and TMP were investigated on the basis of N₂ adsorption–desorption isotherms. The isotherms exhibit type-I isotherms with steep N₂ uptake at a low relative pressure of 0 < P/P₀ < 0.1, reflecting microporosity.^{4,44,46} Also, the presence of H4-type hysteresis (0.1 < P/P₀ < 0.9) suggests the rich existence of mesopores.^{8,38} Moreover, the isotherms with steep N₂ uptake at 0.9 < P/P₀ < 1.0 indicate the macroporosity. Thus, the N₂ adsorption–desorption isotherms in Fig. S1 and S2 (ESI[†]) show PBP1 with rich mesopores, PBP2 and PBP4 mainly with macropores, PBP3, PBP5, PBP6, and PBP8 with rich micropores and mesopores, PBP7 mainly with mesopores and TMP with rich micropores. The BET surface areas were calculated using the P/P₀ values ranging from 0.05 to 0.35: 997 m² g⁻¹ (PBP1), 614 m² g⁻¹ (PBP3), 865 m² g⁻¹ (PBP5), 725 m² g⁻¹ (PBP6), 756 m² g⁻¹ (PBP8) and 629 m² g⁻¹ (TMP) are larger than 31 m² g⁻¹ (PBP2), 32 m² g⁻¹ (PBP4) and 192 m² g⁻¹ (PBP7). Despite PBP8 and TMP are similar in co-monomer structure and specific surface area, the heteroatom distribution and pore size distribution of PBP8 (rich in both micropores and mesopores: 0.77 nm and 2.43 nm) (Fig. S2b and d, ESI[†]) are superior to those of TMP (only rich in micropores: 0.5 nm, 0.85 nm and 1.15 nm). Besides, it has been reported that proper pore size distribution (2–50 nm) of support and proper palladium nanoparticle size (<10 nm) distribution of the highly active sites are helpful for improving the catalyst performance.^{47,48}

The structure effect of co-monomers on the morphology and microstructure of PBPs is shown in Fig. S3 and S4 (ESI[†]). The SEM images of phenanthroline-based polymers, except PBP8, display similar morphology with the variation of co-monomers. It is PBP8 from 1,10-phenanthroline and tetraphenylmethane copolymerization that shows a nanotube morphology, while the others display morphologies of stacked nanosheets. As revealed in TEM analysis, PBP8 (Fig. 2a) and Pd/PBP8 (Fig. 2b) display tubular morphologies, and the outer and inner diameters of the tubes are *ca.* 100 nm and 11 nm, respectively. There are four Pd nanoparticles with an average size of 3 nm in the Pd/PBP8-fresh catalyst (as shown in the red ring of Fig. 2b), indicating that a part of Pd(II) was reduced to Pd nanoparticles during the synthesis of Pd/PBP8, which may be attributed to the electron-donating properties of PBP8. Besides, there are five

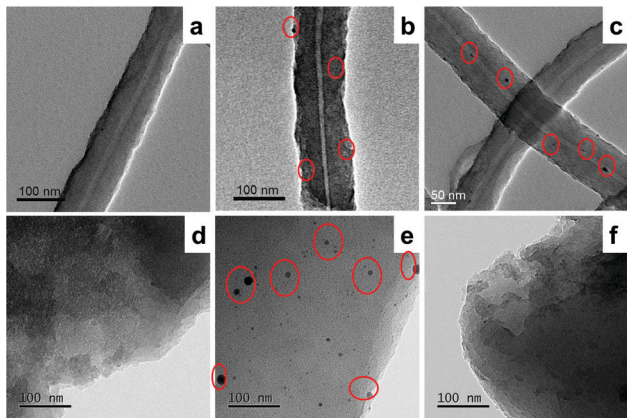


Fig. 2 TEM images of (a) PBP8, (b) Pd/PBP8-fresh, (c) Pd/PBP8-1st used, (d) TMP, (e) Pd/TMP-fresh and (f) Pd/TMP-1st used.

Pd nanoparticles with an average size of 4 nm in the Pd/PBP8-used catalyst (as shown in the red ring of Fig. 2c), indicating that another part of Pd(II) was reduced to Pd nanoparticles in SMRs.

To confirm the successful synthesis of PBP8, ^{13}C -NMR and FT-IR spectra were collected. As shown in Fig. S5 (ESI †), the chemical shift at 39, 63 and 190 ppm can be attributed to C1, C2, and C6 in the tetraphenylmethane, methylene and phenanthroline blocks, respectively,^{5,8,38} suggesting the successful linking of tetraphenylmethane and phenanthroline by methylene. Compared to the FT-IR spectra of 1,10-phenanthroline and tetraphenylmethane, the new peaks at 2850 cm^{-1} and 2930 cm^{-1} detected over PBP8 (Fig. S6, ESI †) can be attributed to the methylene groups,³⁸ again indicating the successful connection of 1,10-phenanthroline and tetraphenylmethane by methylene *via* Friedel-Crafts polymerization. Thermogravimetric analysis (Fig. S7, ESI †) revealed that PBP8 is thermally stable up to $280\text{ }^\circ\text{C}$. The residual mass at $850\text{ }^\circ\text{C}$ was 15.1%, indicating the high carbonization efficiency of PBP8 in an inert atmosphere. The XRD pattern of PBP8 displays a broad peak at 21° (Fig. S8, ESI †), suggesting that PBP8 is amorphous in nature.

To find out the merit of nanotube morphology on catalytic performance, we selected PBP8 to support Pd to generate the Pd/PBP8 catalyst. The fixed pincer-like pyridine nitrogen atoms in 1,10-phenanthroline can coordinate with cations, giving a *cis*-chelating structure.³³ The Pd-catalysed SMR, which is a powerful tool to construct C–C bonds in organic synthesis, was used as the model reaction to investigate the performance of Pd/PBP8. As seen in Fig. S4a and b (ESI †), the nanotube morphology of PBP8 remained after the loading of Pd (0.14 wt.%). Besides, both Pd/PBP8-fresh (Fig. S4b, ESI †) and Pd/PBP8-1st used (Fig. S4c, ESI †) samples have similar nanotube morphology. The results of SEM suggest that the structure of PBP8 is stable.

According to the mechanism of SMRs, the type and solubility of bases strongly affect the SMRs, because bases act as both the co-reactant and promoting agent to initiate the *trans*-metalation step and promote the reductive elimination step, respectively.^{32,33,49} Therefore, it is necessary to conduct optimization experiments

before performance investigation. As listed in Table S2 (ESI †), upon changing the bases as a single variable, Pd/PBP8 exhibited the best activity (78%) when $\text{K}_3\text{PO}_4 \cdot 3\text{H}_2\text{O}$ was used as a base in ethanol–water solution ($V_{\text{EtOH}}:V_{\text{H}_2\text{O}} = 3:2$) at $30\text{ }^\circ\text{C}$ in air (Table S2, ESI † , entries 1–7). To promote reactivity, solvents or mixtures of solvents of medium polarity are often used to dissolve bases and organic reactants. Due to phenylboronic acid derivatives and bases with good hydrophilicity and aromatic halogen derivatives with good lipophilicity, the influence of mixed solvents of water and different organic solvents (entries 7–14) and mixed solvents of different ratios of water and ethanol (entries 15–18) on SMRs yields has been studied (Table S2, ESI †). Across the screened solutions, Pd/PBP8 achieved the highest activity in an ethanol–water mixture when the volume ratio of water-to-organic solvent was 2:3 (entry 7). Additionally, the volume ratio of ethanol and water was also screened (entries 15–18), and Pd/PBP8 exhibited even better activity when the water-to-ethanol volume ratio was 3:2. In the absence of a base or catalyst, no biphenyl product was detected (entries 3 and 19), indicating the necessity of a base and catalyst in the synthesis of biphenyl products.³⁰ As depicted in Table S3 (ESI †), Pd/PBP8 with a nanotube morphology exhibits a high TOF value (3077 h^{-1}) under optimized reaction conditions.

According to the literature,^{51–55} the heterogeneity of the catalyst is usually evaluated by investigating the leaching behaviour in the catalytic reaction. To some extent, the heterogeneity of the catalyst in the SMRs could be confirmed by separated soluble Pd and solid Pd species at a certain time after the reaction started. If the SMRs were catalysed on the surface of solid Pd species, the yield of the reaction will not increase with time delay once the solid Pd species were removed. At the same time, in our work, when the conversion of bromobenzene was around 58%, the Pd/PBP8 catalyst was removed from the reaction system and the mother liquids continued to react for another 3 h. The result exhibited that there was no significant change in either the bromobenzene conversion or the product yield. Besides, after 0.5 h of the reaction, the Pd/PBP8 catalyst removed from the reaction system was washed with water, ethanol and dichloromethane successively and the Pd content of the Pd/PBP8 catalyst was 0.14% as measured by AAS, which was consistent with that of the fresh Pd/PBP8 catalyst. In the above mother liquids, no Pd was detected by ICP-OES, indicating that no Pd species were leached from the Pd/PBP8 catalyst. Thus, we can conclude that the catalysis on the Pd/PBP8 catalyst is indeed heterogeneous in nature.

After having the reaction conditions optimized, the Pd/PBP8 catalyst was tested for SMRs of different substrates and the results are summarized in Table 1. The phenyl-boronic acids substituted with electron-donating (entries 2, 3, 6, 7, 8 and 9) or electron-withdrawing groups (entries 1, 4, 5 and 10) afford excellent yields in the coupling with bromobenzene (80–98%, Table 1, entries 1–10) in 5–12 h at room temperature. To demonstrate the universality of the Pd/PBP8 catalyst for SMRs, the coupling of aryl bromide derivatives with phenylboronic acid was conducted. As shown in Table 1 (entries 11–15), the *ortho*-, *meta*- and *para*-substituted bromobenzenes with electron-donating groups (such as $-\text{CH}_3$ and) achieved high yields

Table 1 Suzuki–Miyaura reaction catalysed by Pd/PBP8^a

Entry	Reactant 1	Reactant 2	Temperature (°C)	Time (h)	Yield ^b (%)	TOF ^d (h ⁻¹)
1			30	5	96	1478
2			30	7	97	1066
3			30	7	96	1055
4			30	5	97	1492
5			30	5	96	1478
6			30	6	98	1256
7			30	6	97	1244
8			30	5	97	1492
9			30	12	80	513
10			30	5	94	1446
11			30	9	98	838
12			30	9	99	846
13			70	13.5	98	558
14			30	9	97	829
15			30	9	98	838
16			70	13.5	97	553
17 ^c			90	15	87	45
18 ^c			90	15	98	503
19 ^c			90	15	99	508
20 ^c			90	15	95	487

^a Pd % = 0.013 mol% of catalyst, 0.5 mmol of aryl halide, 0.75 mmol of arylboronic acid, 1.5 mmol of base (K₃PO₄·H₂O), 3 mL of mixture solvent (V_{H₂O}:V_{ethanol} = 3:2), in air. ^b Isolated yield. ^c 90 °C, 15 h, in Ar. ^d The TOF value from the beginning of the reaction until it reaches equilibrium.

(>97%) after 9 h of reaction at room temperature. Generally, the coupling of phenylboronic acid and bromobenzene derivatives with electron-withdrawing groups requires a high reaction temperature or long reaction time to obtain satisfactory performance.³⁰ For example, 4-hydroxy-bromobenzene afforded 98% yield at 70 °C in 13.5 h (Table 1, entry 16), and 4-nitro-substituted bromobenzene obtained 98% yield at 90 °C in 15 h (Table 1, entry 18). As for 2-nitrobromobenzene, the product yield was 87% at 90 °C in 15 h, plausibly due to the combined effects of electron-withdrawing groups and steric hindrance (Table 1, entry 17). In SMRs, the dissociation of C–Cl bonds is more difficult than

that of C–Br. Therefore, the coupling of chlorobenzene is more difficult than that of bromobenzene. Nevertheless, chlorobenzene and chloromethylbenzene give product yields of 99% and 95% at 90 °C in 15 h, respectively (Table 1, entries 19 and 20). Compared with some reported Pd catalysts, the Pd/PBP8 catalyst shows excellent catalytic performance in SMRs.^{56,60,61} Besides, the ¹H-NMR spectra of the target products in Table 1 are shown in Fig S9 (ESI[†]), which proved that SMRs went successfully with the Pd/PBP8 catalyst.

Although the mechanism of SMRs involves a three-step cycle of oxidative addition, transmetalation and reductive elimination,

the oxidation addition reaction of aryl halide on the Pd(0) surface plays a key role in SMRs.^{32,53,57–59} To illustrate the change of the Pd/PBP8 catalyst before and after the reaction, TEM and XPS were used to analyse the morphology and chemical state, respectively. As shown in Fig. 2b and c, in the TEM images of both the fresh Pd/PBP8 catalyst and the Pd/PBP8-1st used, there are several black spherical particles of size 2–5 nm (in the red ring) that dispersed in the tubular polymer. In the XPS investigation shown in Fig. 3a, the two Pd 3d peaks at 335.9 eV and 341.2 eV can be attributed to the Pd(0) species, while those at 338.1 eV and 343.1 eV to the Pd(II) species.³⁰ The fitting results reveal that there is 59.9 atom% of Pd(0) species in the fresh Pd/PBP8 catalyst. It is deduced that the black spots observed in Fig. 2b (~2 nm) and Fig. 2c (~3 nm) could be related to the palladium nanoparticles^[48]. In the synthesis of fresh Pd/PBP8, the reduction of Pd(II) ions to Pd(0) species may be attributed to the electron-donating ability of the phenanthroline-based support.⁵⁰

As shown in Fig. 3a, there is an increase of Pd(0) species from 59.9% of the fresh Pd/PBP8 to 79.4% after 7 cycles of reaction, which may be the result of the reduction of Pd(II) by phenylboronic acid during the SMRs.^{61,62} Meanwhile, after being reused 7 times (Fig. 4), the Pd/PBP8 catalyst only showed a slight decrease of 4.2% in activity, implying good recyclability. According to the results of AAS, the change of the Pd content between Pd/PBP8-fresh and Pd/PBP8-used (for 7 times) is insignificant, both with a value of *ca.* 0.14 wt.%. The results clearly indicate that the Pd species are firmly anchored on the

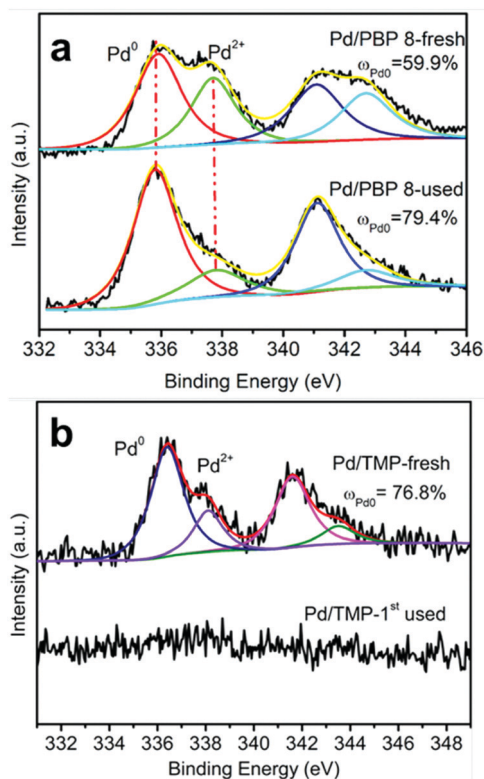


Fig. 3 XPS Pd 3d spectra of (a) Pd/PBP8-fresh and Pd/PBP8-used and (b) Pd/TMP-fresh and Pd/TMP-1st used.

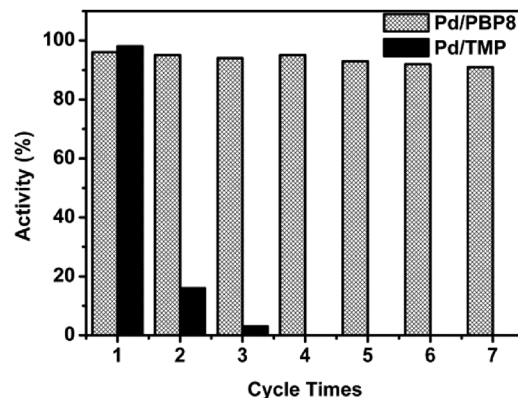


Fig. 4 Catalytic activity of Pd/PBP8 and Pd/TMP in 7 cycles of SMRs.

1,10-phenanthroline units and there is almost no Pd leaching during the reaction. The N atoms in the phenanthroline monomer can form a stable chelate with metal ions like a crab's tongs to adsorb the metal ions, and the framework of the organic porous material can confine the palladium nanoparticles. These two effects can inhibit the loss of palladium active species (including metal ions and nanoparticles). Catalysed by the Pd/PBP8-fresh and Pd/PBP8-7th used catalysts, the SMR of bromobenzene and phenylboronic acid gave yields of 97% and 93% within 5 h at 30 °C, respectively. The above results indicate that the Pd/PBP8 catalyst has good catalytic performance which is not inferior to that reported in the literature (listed in Table S5, ESI[†]).

Compared to Pd/PBP8, Pd/TMP gives a higher product yield (Table S3, ESI[†]) in the first cycle but with much poorer recyclability (Fig. 4), which is mainly due to Pd leaching. Without the help of heteroatoms for palladium anchoring, there is an aggregation (see in the red ring of Fig. 2e) and leaching (Fig. 2f) of the Pd nanoparticles. In addition, the XPS spectrum of the "Pd/TMP-1st used" sample exhibited no Pd 3d peaks, indicating the near-complete loss of the surface Pd species (Fig. 3b). Because TMP and PBP8 were synthesized by the polymerization of tetraphenylmethane with phenanthrene and 1,10-phenanthroline, respectively, it can be deduced that the excellent reusability of Pd/PBP8 is mainly due to the inclusion of the heteroatom N in the PBP8 structural unit.

4. Conclusion

In summary, a series of PBPs were synthesized by a one-pot Friedel-Crafts polymerization method. Among them, most of the PBPs displayed a nanosheet morphology, except PBP8 which displayed both one-dimensional nanotubular morphology and a large surface area of 745 m² g⁻¹. Due to the presence of N atoms in the structural units of PBP8, the Pd nanoparticles (size 2–5 nm) reduced from Pd(II) were highly dispersed in the PBP8 nanotube in the synthesis of Pd/PBP8 (as shown in the TEM image). At room temperature and in aqueous solutions, Pd/PBP8 catalyzed the SMRs of bromobenzene and 10 benzenboric acid derivatives, respectively, and all their yields were more than 80%

in 7 hours, suggesting the outstanding catalytic performance of Pd/PBP8 in aqueous SMRs under ambient conditions. Moreover, the combined data analysis of the hot filtration test and elemental analyses strongly pointed towards a heterogeneous system. This work presents a simple method for the fabrication of polymer nanotubes which may find wide applications in other fields such as sorption and energy storage.

Conflicts of interest

There are no conflicts to declare.

Acknowledgements

This work was supported by the PhD Start-Up Fund (30002/2042019026) for Young Teachers of Huanggang Normal University.

Notes and references

- Q. Chang, R. Wang, J. Wang, Y. Muhammad, Z. Zhao, Z. Feng, Z. Huang, Y. Zhang and Z. Zhao, Nitrogen-doped hollow copolymer tube via template-free asynchronous polymerization with highly selective separation of hydrophilic dipeptide for enhancing inhibitory activity of angiotensin converting enzyme, *ACS Appl. Mater. Interfaces*, 2019, **11**(35), 31700–31708.
- Y. Liu, B. Housseinou, D. Nguyen, O. Ersen, T. Romero, S. Zafeiratos, D. Bégin, I. Janowska and P. H. Cuong, Synthesis of porous carbon nanotubes foam composites with a high accessible surface area and tunable porosity, *J. Mater. Chem. A*, 2013, **1**(33), 9508–9516.
- X. Li, H. Xiong and Q. Jia, A Versatile solvent-induced polymerization strategy to synthesize free-standing porous polymer nanosheets and nanotubes for fast iodine capture, *ACS Appl. Mater. Interfaces*, 2019, **11**(49), 46205–46211.
- W. Fan, X. Liu, Z. Zhang, Q. Zhang, W. Ma, D. Tan and A. Li, Conjugated microporous polymer nanotubes and hydrophobic sponges, *Microporous Mesoporous Mater.*, 2014, **196**, 335–340.
- A. Modak, P. Bhanja and A. Bhaumik, Microporous nanotubes and nanospheres with iron-catechol sites: efficient Lewis acid catalyst and support for Ag nanoparticles in CO₂ fixation reaction, *Chem. – Eur. J.*, 2018, **24**(53), 14189–14197.
- Z. Yang, Z. Liu, H. Zhang, B. Yu, Y. Zhao, H. Wang, G. Ji, Y. Chen, X. Liu and Z. Liu, N-Doped porous carbon nanotubes: synthesis and application in catalysis, *Chem. Commun.*, 2017, **53**(5), 929–932.
- Z. Zhu, Z. Yang, Y. Fan, C. Liu, H. Sun, W. Liang and A. Li, Calcination of porphyrin-based conjugated microporous polymers nanotubes as nanoporous N-rich metal-free electrocatalysts for efficient oxygen reduction reaction, *ACS Appl. Energy Mater.*, 2020, **3**(6), 5260–5268.
- Y. Chen, H. Sun, R. Yang, T. Wang, C. Pei, Z. Xiang, Z. Zhu, W. Liang and A. Li, Synthesis of conjugated microporous polymer nanotubes with large surface areas as absorbents for iodine and CO₂ uptake., *J. Mater. Chem. A*, 2015, **3**(1), 87–91.
- J. Lee and J. Y. Chang, Synthesis and functionalization of ynone-based tubular microporous polymer networks and their carbonized products for CO₂ capture, *Macromol. Res.*, 2019, **27**(10), 1–7.
- P. Mu, W. Ma, Y. Zhao, C. Zhang, S. Ren, F. Wang, C. Yan, J. H. Zeng and J. Jiang, Facile preparation of MnO/nitrogen-doped porous carbon nanotubes composites and their application in energy storage, *J. Power Sources*, 2019, **426**, 33–39.
- Y. Zhao, W. Wu, J. Li, Z. Xu and L. Guan, Encapsulating MWNTs into hollow porous carbon nanotubes: a tube-in-tube carbon nanostructure for high-performance lithium-sulfur batteries., *Adv. Mater.*, 2014, **26**(30), 5113–5118.
- S. Lei, X. Cui, X. Liu, X. Zhang, X. Han and Y. Yang, Hydrothermally self-templated synthesis of rectangular polyimide submicrotubes and promising potentials in electrochemical energy storage, *Chem. Commun.*, 2020, **56**(9), 1429–1432.
- Z. He, T. Wang, Y. Xu, M. Zhou, W. Yu, B. Shi and K. Huang, Construction of microporous organic nanotubes based on scholl reaction, *J. Phys. Chem. C*, 2018, **122**(16), 8933–8940.
- R. R. Haikal, A. B. Soliman, M. Amin, S. Karakalos, Y. S. S. Hassan, A. M. Elmansi, I. H. Hafez, M. R. Berber, A. Hassanien and M. H. Alkordi, Synergism of carbon nanotubes and porous-organic polymers (POPs) in CO₂ fixation: one-pot approach for bottom-up assembly of tunable heterogeneous catalyst, *Appl. Catal., B*, 2017, **207**, 347–357.
- W. Ming, S. Bi, Y. Zhang, K. Yu, C. Lu, X. Fu, F. Qiu, P. Liu, Y. Su and F. Zhang, Bottom-up preparation of fully sp²-bonded porous carbons with high photoactivities, *Adv. Funct. Mater.*, 2019, **29**(14), 1808423.
- J. Wang, Z. Yang, M. Ahmad, H. Zhang, Q. Zhang and B. Zhang, A novel synthetic method for tubular nanofibers, *Polym. Chem.*, 2019, **10**(31), 4239–4245.
- Q. Gao, L. Bai, X. Zhang, P. Wang, P. Li, Y. Zeng and R. Zou, Synthesis of microporous nitrogen-rich covalent-organic framework and Its application in CO₂ capture, *Chin. J. Chem.*, 2015, **33**(001), 90–94.
- X. Feng, Y. Liang, L. Zhi, A. Thomas, D. Wu, I. Lieberwirth, U. Kolb and K. Müllen, Synthesis of microporous carbon nanofibers and nanotubes from conjugated polymer network and evaluation in electrochemical capacitor, *Adv. Funct. Mater.*, 2009, **19**(13), 2125–2129.
- J. Chun, J. H. Park, J. Kim, S. M. Lee, H. J. Kim and S. U. Son, Tubular-shape evolution of microporous organic networks, *Chem. Mater.*, 2012, **24**(17), 3458–3463.
- X. Liang, Y. Liu, Z. Wen, L. Huang, X. Wang and H. Zhang, A Nano-structured and highly ordered polypyrrole-sulfur cathode for lithium-sulfur batteries, *J. Power Sources*, 2011, **196**(16), 6951–6955.
- Y. Wang, W. Song, M. Li and Z. Wu, Oxygen reduction reaction mechanisms on heteroatom-doped single-walled

- carbon nanotube catalysts: insights from a theoretical study, *J. Electrochem. Soc.*, 2019, **166**(10), F670–F678.
- 22 L. Li, Y. M. Zhou, R. Y. Gao, X. C. Liu, H. H. Du, J. L. Zhang, X. C. Ai, J. P. Zhang, L. M. Fu and L. H. Skibsted, Naturally occurring nanotube with surface modification as biocompatible, target-specific nanocarrier for cancer phototherapy, *Biomaterials*, 2019, **190**, 86–96.
 - 23 S. B. Kandy, G. P. Simon, W. Cheng, J. Zank, K. Saito and A. R. Bhattacharyya, Effect of organic modification on multiwalled carbon nanotube dispersions in highly concentrated emulsions., *ACS Omega*, 2019, **4**(4), 6647–6659.
 - 24 S. Hu, Y. Xu, J. Wang, P. Zhang and J. Guo, Modification effects of carbon nanotube dispersion on the mechanical properties, pore structure, and microstructure of cement mortar, *Materials*, 2020, **13**(5), 1101–1116.
 - 25 S. Qu, Q. Yao, L. Wang, J. Hua and L. Chen, A novel hydrophilic pyridinium salt polymer/SWCNTs composite film for high thermoelectric performance, *Polymer*, 2018, **136**(31), 149–156.
 - 26 G. Stando, D. Lukawski, F. Lisiecki and D. Janas, Intrinsic hydrophilic character of carbon nanotube networks, *Appl. Surf. Sci.*, 2019, **463**, 227–233.
 - 27 J. S. Appasamy, J. C. Kurnia and M. K. Assadi, Synthesis and evaluation of nitrogen-doped titanium dioxide/single walled carbon nanotube-based hydrophilic self-cleaning coating layer for solar photovoltaic panel surface, *Sol. Energy*, 2020, **196**, 80–91.
 - 28 C. Huettner, D. Hagemann, E. Troschke, F. Hippauf, L. Borchardt, S. Oswald, T. Henle and S. Kaskel, Tailoring the adsorption of ACE-inhibiting peptides by nitrogen functionalization of porous carbons, *Langmuir*, 2019, **35**(30), 9721–9731.
 - 29 S. J. Kraft, R. H. Sánchez and A. S. Hock, A remarkably active iron catecholate catalyst immobilized in a porous organic polymer, *ACS Catal.*, 2013, **3**(5), 826–830.
 - 30 J. Cookson, The Preparation of Palladium Nanoparticles, *Platinum Met. Rev.*, 2012, **56**(2), 83–98.
 - 31 A. Gao, R. Lu and G. Veser, Stabilizing metal nanoparticles for heterogeneous catalysis, *Phys. Chem. Chem. Phys.*, 2010, **12**, 13499–13510.
 - 32 B. V. Vaerenbergh, J. Lauwaert, P. Vermeir, J. W. Thybaut and J. D. Clercq, Towards high-performance heterogeneous palladium nanoparticle catalysts for sustainable liquid-phase reactions, *React. Chem. Eng.*, 2020, **5**, 1556–1618.
 - 33 J. Chen, J. Zhang, Y. Zhang, M. J. Xie and T. Li, Nanoporous phenanthroline polymer locked Pd as highly efficient catalyst for Suzuki–Miyaura Coupling reaction at room temperature, *Appl. Organomet. Chem.*, 2020, **34**(2), e5310.
 - 34 S. S. Soomro, C. Röhlich and K. Köhler, Suzuki Coupling Reactions in pure water catalyzed by supported palladium—relevance of the surface polarity of the support, *Adv. Synth. Catal.*, 2011, **353**, 767–775.
 - 35 G. H. Gunasekar and S. Yoon, A phenanthroline-based porous organic polymer for the iridium-catalyzed hydrogenation of carbon dioxide to formate, *J. Mater. Chem. A*, 2019, **7**, 14019–14026.
 - 36 C. A. Wang, K. Nie, G. D. Song, Y. W. Li and Y. F. Han, Phenanthroline-based microporous organic polymer as a platform for an immobilized palladium catalyst for organic transformations, *RSC Adv.*, 2019, **9**(15), 8239–8245.
 - 37 J. Y. Yue, L. Wang, L. Zhang, Y. Ma, P. Yang and B. Tang, Phenanthroline-functionalized porous aromatic framework: An efficient heterogeneous catalyst for the tandem reaction of 2-iodoanilines and isothiocyanates in water, *Microporous Mesoporous Mater.*, 2020, **305**, 110313.
 - 38 C. W. kang, J. H. Ko, S. M. Lee, H. J. Kim, Y. J. Ko and S. Son, Noncovalent and covalent double assembly: unravelling a unified mechanism for the tubular shape evolution of microporous organic polymers, *J. Mater. Chem. A*, 2019, **7**(13), 7859–7866.
 - 39 H. Yu and R. Haner, Solution phase synthesis of 1D tubular polymers via preorganization-polymerization, *Chem. Commun.*, 2016, **52**, 14396–14399.
 - 40 L. Bao, H. Sun, Z. Zhu, W. Liang, P. Mu, J. Zang and A. Li, Synthesis and properties of tubular-shape conjugated microporous polymers with high purity, *Mater. Lett.*, 2016, **178**, 5–9.
 - 41 I. Agranat, Y. N. Oded, T. Malábi, S. Pogodin and S. Cohen, The linkage between reversible Friedel–Crafts acyl rearrangements and the Scholl reaction, *Struct. Chem.*, 2019, **30**, 1579–1610.
 - 42 J. T. Soe, P. Puthiaraj and W. S. Ahn, AlCl₃-catalyzed synthesis of tetraphenylsilane-based hyper cross-linked organic polymers for CO₂ adsorption, *Adv. Porous Mater.*, 2016, **4**(2), 118–124.
 - 43 Q. Wang, H. Gao, Q. Cui, K. Wu, F. Hao, J. Yu, Y. Zhao and Y. U. Kwon, Improving lithium–sulfur battery performances by using conjugative porous polymer as the sulfur support: the case of N-containing porous aromatic framework, *J. Solid State Electrochem.*, 2019, **23**, 657–666.
 - 44 J. Xu, J. Ou, L. Chen, H. Zhang, S. Ma and M. L. Ye, Palladium catalyst imbedded in polymers of intrinsic microporosity for the Suzuki–Miyaura coupling reaction, *RSC Adv.*, 2018, **8**(61), 35205–35210.
 - 45 B. Li, Z. Guan, W. Wang, X. Yang, J. Hu, B. Tan and T. Li, Highly dispersed Pd catalyst locked in knitting aryl network polymers for Suzuki–Miyaura coupling reactions of aryl chlorides in aqueous media, *Adv. Mater.*, 2012, **24**, 3390–3395.
 - 46 M. Kim, E. Yoo, W. S. Ahn and S. E. Shim, Controlling porosity of porous carbon cathode for lithium oxygen batteries: Influence of micro and meso porosity, *J. Power Sources*, 2018, **389**, 20–27.
 - 47 P. Munnik, P. E. Jongh and K. P. Jong, Recent developments in the synthesis of supported catalysts, *Chem. Rev.*, 2015, **115**(14), 6687–6718.
 - 48 B. V. Vaerenbergh, J. Lauwaert, P. Vermeir and J. D. Clercq, and 46 Thybaut, J. W., Chapter one-synthesis and support interaction effects on the palladium nanoparticle catalyst characteristics, *Adv. Catal.*, 2019, **65**, 1–120.
 - 49 C. Amatore, G. L. Duc and A. Jutand, Mechanism of Palladium-Catalyzed Suzuki–Miyaura Reactions: Multiple

- and Antagonistic Roles of Anionic “Bases” and Their Counterions, *Chem. – Eur. J.*, 2013, **19**, 10082–10093.
- 50 S. Y. Ding, J. Gao, Q. Wang and Y. Zhang, Construction of Covalent Organic Framework for Catalysis: Pd/COF-LZU1 in Suzuki-Miyaura Coupling Reaction, *J. Am. Chem. Soc.*, 2011, **133**, 19816–19822.
- 51 B. V. Vaerenbergh, J. Lauwaert, J. W. Thybaut, P. Vermeir and J. D. Clercq, Pd nanoparticle and molecular Pd²⁺ leaching pathways for a strongly acid *versus* strongly basic resin supported Pd nanoparticle catalyst in Suzuki coupling, *Chem. Eng. J.*, 2019, **374**, 576–588.
- 52 M. Ródenas, J. E. Haskouri, J. V. Ros-Lis, M. D. Marcos, P. Amorós, M. A. Úbeda and F. Pérez-Pla, Highly active hydrogenation catalysts based on Pd nanoparticles dispersed along hierarchical Porous Silica covered with polydopamine as interfacial glue, *Catalysts*, 2020, **10**(4), e449.
- 53 B. Sun, L. Ning and H. C. Zeng, Confirmation of Suzuki-Miyaura cross-coupling reaction mechanism through synthetic architecture of nanocatalysts, *J. Am. Chem. Soc.*, 2020, **142**(32), 13823–13832.
- 54 J. M. Richardson and C. W. Jones, Strong evidence of solution-phase catalysis associated with palladium leaching from immobilized thiols during Heck and Suzuki coupling of aryl iodides, bromides, and chlorides, *J. Catal.*, 2007, **251**, 80–91.
- 55 M. V. Polynski and V. P. Ananikov, Modeling Key Pathways Proposed for the Formation and Evolution of “Cocktail”-Type Systems in Pd-Catalyzed Reactions Involving ArX Reagents, *ACS Catal.*, 2019, **9**(5), 3991–4005.
- 56 W. Fu, Y. Cao, Q. Feng, W. R. Smith, P. Dong, M. Ye and J. Shen, Pd-Co nanoalloys nested on CuO nanosheets for efficient electrocatalytic N₂ reduction and room-temperature Suzuki-Miyaura coupling reaction, *Nanoscale*, 2019, **11**, 1379–1385.
- 57 M. García-Melchor, A. C. Braga, A. Lledós, G. Ujaque and F. Maseras, Computational perspective on Pd-catalyzed C–C cross-coupling reaction mechanisms, *Acc. Chem. Res.*, 2013, **46**(11), 2626–2634.
- 58 T. Yaman and J. N. Harvey, Suzuki-Miyaura coupling revisited: an integrated computational study, *Faraday Discuss.*, 2019, **220**, 425–442.
- 59 A. J. J. Lennox and G. C. Lloyd-Jones, Transmetalation in the Suzuki-Miyaura Coupling: The Fork in the Trail, *Angew. Chem., Int. Ed.*, 2013, **52**, 7362–7370.
- 60 J. Chen, J. Zhang, D. Zhu and T. Li, Porphyrin-based polymer-supported palladium as an excellent and recyclable catalyst for Suzuki-Miyaura coupling reaction in water, *Appl. Organomet. Chem.*, 2017, **32**(2), e3996.
- 61 S. S. Soomro, F. L. Ansari, K. Chatziapostolou and K. Köhler, Palladium leaching dependent on reaction parameters in Suzuki-Miyaura coupling reactions catalyzed by palladium supported on alumina under mild reaction conditions, *J. Catal.*, 2010, **2**(273), 138–146.
- 62 G. Collins, M. Schmidt, C. O’Dwyer, J. D. Holmes and G. P. McGlacken, The Origin of Shape Sensitivity in Palladium-Catalyzed Suzuki-Miyaura Cross Coupling Reactions, *Angew. Chem., Int. Ed.*, 2014, **53**(16), 4142–4145.